Available online at www.sciencedirect.com

jmr&t Journal of Materials Research and Technology

journal homepage: www.elsevier.com/locate/jmrt

Original Article

Effect of powder recycling on inclusion content and distribution in AISI 316L produced by L-PBF technique

A. Lanzutti [a,*], F. Sordetti [a], R. Montanari [b], A. Varone [b,**], E. Marin [c], F. Andreatta [a], S. Maschio [a], E. Furlani [a], M. Magnan [a], E. Vaglio [a], E. Pakhomova [d], M. Sortino [a], G. Totis [a], L. Fedrizzi [a]

[a] University of Udine, Polytechnic Department of Engineering and Architecture, Via Delle Scienze 208, 33100 Udine, Italy

[b] Department of Industrial Engineering, University of Rome "Tor Vergata", Via Del Politecnico 1, 00133 Rome, Italy

[c] Kyoto Institute of Technology, Kyoto, Japan

[d] Università di Cagliari, Dipartimento di Ingegneria Meccanica, Chimica e Dei Materiali, Via Marengo 2, 09123 Cagliari, Italy

ARTICLE INFO

Article history:
Received 4 November 2022
Accepted 3 February 2023
Available online 8 February 2023

Keywords:
AISI 316 L
L-PBF
Microstructure
Inclusions
Powder recycling

ABSTRACT

AISI 316 L stainless steel is widely used as material to produce components by means of additive manufacturing. To increase the circular economy, the powders are collected and re-used after the printing process, thus the effect of powder recycling on microstructure and properties of printed components is of the utmost importance. This work focused the attention on non-metallic inclusions by examining virgin and recycled powders, and products printed by using both types of powders in a laser powder bed fusion (L-PBF) process.

Recycled powders exhibit an irregular shape due to fragmentation, spatters and satellites and, compared to the virgin ones, have a higher gas (O, H and C) content. Both powders contain non-metallic inclusions with a larger quantity in the recycled ones.

The printed samples have a similar microstructure, however those produced by using recycled powders exhibit voids of larger size and a little greater amount of inclusions. XRD and EDS examinations of inclusions extracted from the metallic matrix showed that they consist of a mix of amorphous and crystalline silica. Large part of these particles are already present in virgin powders and only a minor part forms during repeated printing operations. Accordingly, the quality of virgin powders is the factor that mainly affects the inclusion content of printed products indicating that the powder production process is the most critical stage of the whole manufacturing process.

* Corresponding author.
** Corresponding author.
E-mail addresses: alex.lanzutti@uniud.it (A. Lanzutti), alessandra.varone@uniroma2.it (A. Varone).

https://doi.org/10.1016/j.jmrt.2023.02.017

1. Introduction

In recent years, the research of additive manufacturing (AM) processes covered different technological areas aiming to print complex and well-designed components with selected materials. One of the most studied materials is AISI 316 L stainless steel, that is widely used for its excellent corrosion resistance. With respect to the wrought material, AISI 316 L produced by AM processes exhibits improved mechanical properties [1], corrosion resistance [2,3] and also wear resistance [4]. To reach these properties, an important role is played by powder quality that influences some typical defects of AM products [5].

In agreement to the circular economy concept [6], powders are commonly re-used many times and submitted to post processing treatments. Nevertheless, re-used powders present different characteristics than the virgin ones. Lu et al. [7] observed that re-used powders become coarser and their microstructure changes with the effect of increasing O content and non-metallic inclusions in the 3D printed material. In samples produced by Direct Energy Deposition (DED), Saboori et al. [8] proved that a strong decrease of ductility is connected to the presence of inclusions with large size. To overcome the drawback of the irregular morphology, some authors [6,9] proposed to spheroidize the powders before the re-use.

An extensive study was performed by Heiden et al. [10] who evidenced how powder recycling affects many of their features. In detail, they observed an increase of the average diameter, a reduction of powder circularity with the presence of satellites and oxides on the surface, an increase of O content, no other variations of chemical composition, and an increase of delta ferrite content. Some works were focused on the effect of spatters [11,12] that are usually generated by metal projections during laser passes and whose content progressively increases as powders are re-used. Another relevant factor affecting the properties of 3D printed material is the presence of delta ferrite [7,8,13] because it induces an unstable behavior of the laser beam giving rise to internal defects [13]. Therefore, magnetic separation of the powders after some re-using cycles has been suggested to reduce the amount of powders rich of delta ferrite in the feedstock.

Although powder recycling generally leads to a microstructural evolution, controversial results are sometimes reported in literature about its effect on the mechanical properties of printed parts. For instance, Delacroix et al. [14] found no significant difference on micro-hardness and tensile properties of components printed by laser powder bed fusion (L-PBF) with re-used AISI 316 L powders.

A topic of particular interest for industrial applications is the origin of non-metallic inclusions and their effect on the properties of the 3D printed materials (e.g. see Refs. [12,15–18]). The undesired presence of such inclusions may depend on different factors: (i) the interaction of molten metal with O present in the printing chamber [19], (ii) the presence of oxides in virgin powders [12], (iii) incorrect process parameters, and (iv) the presence of de-oxidizing alloying elements. Therefore, it is important to understand the specific role played by each of these factors to improve the quality of products printed in industrial processes.

The inclusions in austenitic stainless steels produced by L-PBF technique are usually of sub-micrometric size and consist of Si–Mn–Mo oxides [20], Si–Mn oxides [7,12], Cr_2O_3/MnO/SiO_2 [15,19], Si–Mn/Cr–Mn oxides [17] and Si–Mn/Si oxides [16]. Sub-micrometric inclusions slightly increase the tensile resistance of the material [15] but are deleterious for toughness and stress corrosion cracking resistance [20]. In particular, Lou et al. [20] observed that inclusions in AISI 316 L steel manufactured by L-PBF promote early initiation of microvoids reducing the impact toughness. Moreover, for stress corrosion cracking in high temperature water, Si-rich inclusions along the grain boundaries preferentially dissolve, accelerate oxidation and cause extensive crack branching.

This work investigates the effect of powder recycling on content and distribution of non-metallic inclusions in AISI 316 L steel printed by L-PBF. The conditions examined in this work are those typical of an industrial process where the re-used powders are mixed with virgin ones after some jobs [21]. Aiming to understand which process parameters mainly affect the content of inclusions in printed materials, virgin and recycled powders, and products manufactured by using both types of powders have been examined by scanning electron microscopy (SEM), energy dispersion spectroscopy (EDS) and trace elements analysis. The nature of inclusions and their relative amounts in printed materials have been determined by extracting the inclusions from the metallic matrix through an electrolytic procedure and examining them by means of EDS and X-ray diffraction (XRD). The output of this work is extremely important because the main aim is to determine the origin of the inclusions in the additively manufactured samples in order to give the necessary information regarding the possible precautions to reduce it. The final goal is to set up the process to increase the quality of the 3D printed material.

2. Experimental setup

2.1. *Powder characterization*

The materials used in this work are virgin AISI 316 L powders, provided by GE additive, and recycled powders extracted from the L-PBF machine after 25 jobs. During this time, the powders were sieved 10 times and new virgin powders were inserted 4 times, obtaining a mixture of virgin powders and re-used powders. The last virgin powder addition was done after the production of the 17th job, while the last sieving process was performed after the production of 23rd job. Before the inspection, the material was sieved one additional time in order to remove the undesired constituents formed during the last processes (e.g. splatters and debris) and bring the powders to the ready-for-use condition, as it was in the case of virgin powders. This is the standard procedure of the laboratory to re-integrate the used powders and substantially corresponds to that commonly used in powder bed fusion practice [21].

Both type of powders were analyzed in order to determine their chemical composition, dimensional distribution, shape, microstructure and content of inclusions. In particular, the chemical composition was acquired by using SEM + EDS probe (Zeiss Evo-40+INCA X-sight), to detect the main alloying

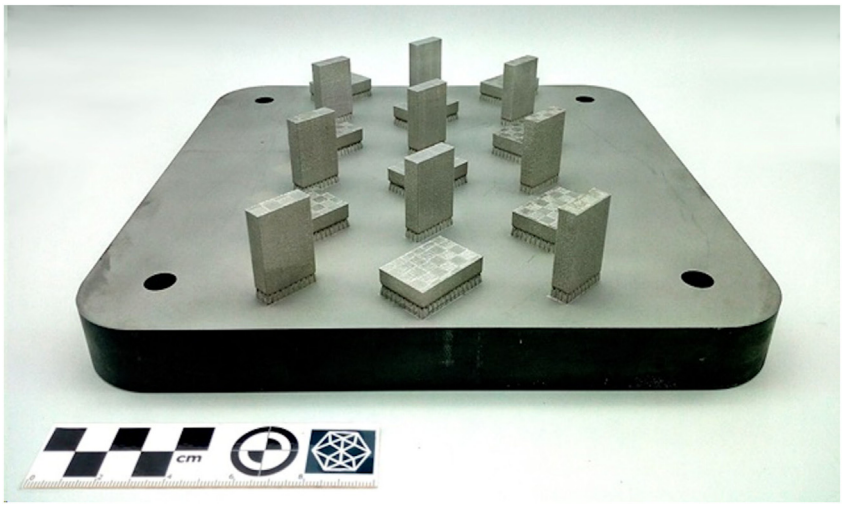

Fig. 1 – Batch of samples produced to investigate the effect of powder recycling on parts produced by L-PBF. The batch in the picture was produced with recycled powders.

elements in the powders, and gas in metal analyzers to determine the content of O, N, C and S. Trace elements analysis (C, O, N, S and H) was performed using an EMIA-Expert Carbon/sulfur analyzer (Horiba Scientific, Kyoto, Japan) and an EMGA-930 Oxygen/Nitrogen/Hydrogen analyzer (Horiba Scientific, Kyoto, Japan). The accuracy for each element was as follows: C and S $\leq$ 0.03 ppm, O and N $\leq$ 0.02 ppm, H $\leq$ 0.04 ppm. For the gas in metal and EDXS analysis, 5 measurements for each batch and analyzed element were performed to ensure adequate reproducibility of the results.

Laser scattering particle size distribution analyzer (Horiba Scientific LA-950) was employed to detect the powder size and its distribution, while the shape was evaluated by SEM analysis (3 measurements for each batch). Part of the powders were embedded in epoxy resin and underwent conventional metallographic preparation. These samples were etched by acetic glyceregia (10 ml nitric acid, 15 ml hydrocloridic acid, 10 ml acetic acid, 2 drop glycerine) and then analyzed by light microscopy and FE-SEM + EDS (Jeol JSM 7610F + INCA Ultimax) to determine the presence of inclusions inside the powder particles. To perform these measurements several images have been acquired and stitched together; the obtained cumulative image was analyzed to determine the density (counts/area), shape and distribution of the inclusions (3 powder grains for each batch).

2.2. *Characterization of printed samples*

In order to investigate the effect of powder deterioration on the parts produced by L-PBF, two identical batches of samples were manufactured using virgin and recycled powders (Fig. 1). Each batch consisted of 18 cuboids (30.5 × 20.5 × 7 mm): 9 oriented with the major surface parallel to the building platform (horizontal) and 9 oriented perpendicularly to it (vertical). The samples were homogeneously arranged on the building platform to avoid any influence related to the position in the printing chamber. The machine used for the experiments was a commercial Concept Laser M2 Cusing equipped with a single-mode CW ytterbium-doped fiber laser with an emission wavelength of 1070 nm. The process was performed in Ar atmosphere with less than 0.2% of residual oxygen.

The main process parameters used for producing the samples are reported in Table 1. The exposure strategy consisted in a checkerboard pattern of 5 × 5 mm squares that were bi-directionally scanned along mutually perpendicular directions (Fig. 2). Adjacent squares were spaced 0.045 mm apart, and each of them underwent an angular shift of 90° and a linear shift of 1 mm in X and Y directions at each layer to promote structural evenness within the processed material.

In an additional job, 10 probes for tensile tests were produced on the vertical printing direction, by using the same parameters. The probe geometry is described in Ref. [22].

At the end of the manufacturing process, the samples were separated from the building platform by using a band saw machine, and the support structures were removed. Afterwards, some samples from each of the two batches were analyzed by glow discharge optical emission spectrometry (RF-GDOES, HR GD Profiler,m Horiba jobin Yvon), to determine their chemical composition, and gas in metal analyser, to determine the O, H, C, S, and N content. A procedure similar to that for the analysis of powders was used for trace elements.

The samples underwent total voids analysis by means of Archimede' weighting method (4 samples for each batch).

Some samples (at least 2) from each of the two batches were then cut by using an abrasive, water-refrigerated wheel.

Table 1 – Process parameters for samples production.

	Bulk area	Supports
Power	180 W	130 W
Scanning speed	600 mm/s	1000 mm/s
Spot diameter	120 μm	50 μm
Hatch distance	105 μm	–
Layer thickness	25 μm	50 μm

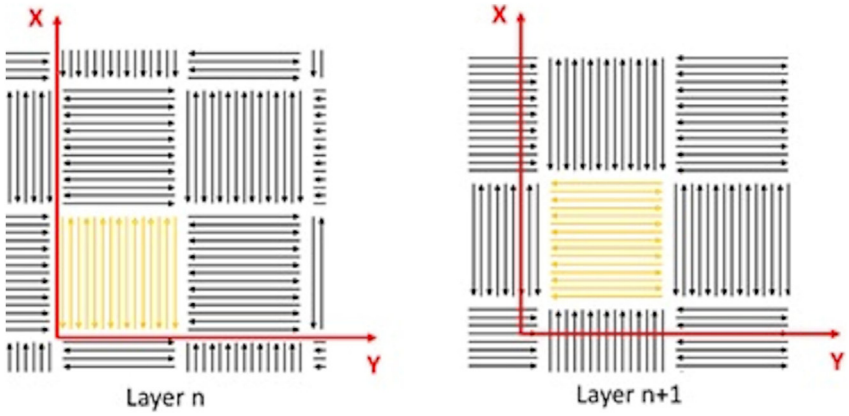

Fig. 2 – Exposure strategy for the sample production.

Thereafter, they were embedded in epoxy resin, and submitted to metallographic preparation to obtain a mirror-like surface. Prior to etching, they were analyzed by light microscopy only in the vertical direction, to determine the pore and voids content. In this case, the procedure was in agreement to the ASTM E–45 standard, which was used to determine the inclusion content in steel specimens. The analysis gave also information on the voids size and distribution on the whole analyzed area. The samples were successively etched by acetic glyceregia for 60 s. Their microstructure was analyzed by light microscopy and FE-SEM + EDS. FE-SEM observations were performed to acquire several micrographs at high magnification that were then stitched together for reconstructing the image of a single melting pot. The images of three melting pots in different positions (top, middle and bottom), taken from a sample printed in vertical direction, were examined by highlighting the inclusions found in the material (indicated by red dots in the images). Afterwards, the image, that is composed by FE-SEM images in gray scale, was colour filtered in order to obtain only the inclusions highlighted in red to make easier the final counting by means of an image analysis software (image J). The number of inclusions was normalized to the analyzed area. The results obtained from samples printed with virgin and recycled powders were compared to highlight possible differences.

Vickers hardness tests (10 HV2 measurements on printed samples for each powder batch) and tensile tests were performed on the samples produced with both types of powders. Tensile tests were performed on 10 probes for each powder batch by means of a universal testing machine MTS 810 in a mixed operation mode: strain control up to 2% of elongation (strain rate of 0.1 mm/min) and displacement control (displacement rate of 1 mm/min) up to the probe fracture.

To extract the inclusions, 3D printed samples of both batches (3 samples for each batch) were completely dissolved by means of an electrolythic procedure: solution of 180 ml of methanol and 20 ml of HCl, cathode of Pt, applied voltage 2.9 V, current 1.3 mA, ambient temperature. Filters with pores of 0.1 μm were used to collect the particles from the bath. The collected particles were successively washed in methanol, dried in air and examined by XRD and EDS. The original samples and the particulate extracted from each sample were weighted to determine the relative amount of non-metallic inclusions.

The XRD patterns of extracted particles were recorded using the Mo-Kα radiation ($\lambda = 0.07093$ nm) in step-scanning mode with angular 2θ steps of 0.05° and counting time per step of 5 s. To identify the compounds present in the extracted particles, the XRD peak positions were compared with those reported in the JCPDS database [23].

3. Results

3.1. *Powder characterization*

The SEM images of the powders used in this work are shown in Fig. 3.

The image in (a) shows that virgin powders are spherical with diameters ranging from few microns to 30–40 μm. In contrast, recycled powders (b) present a higher amount of elongated (not spherical) particles and agglomerated particles. In Fig. 4, displaying recycled powders at higher magnification, particles of irregular shape (a) and with satellites (b) can be observed. Satellites are formed by small metal projections attached on the surface of particles. Moreover, as previously reported by other researchers [11,24,25], some particles are partially coated by metal spatters (b).

By analysing the particles size distribution by means of laser scattering measurements (Fig. 5), it was observed that the virgin powders present a slightly sharper normal distribution of particle sizes. The median diameter of the particles is the same for both the analyzed powders (about 29 μm). Nevertheless, there are fewer particles having the median diameter when considering the recycled powders with respect to the virgin powders. After recycling, the size distribution curve becomes broader because on one side coarsening of a part of the particles takes place due to the partial coating of metal spatters and agglomeration (see Fig. 4), while on the other side some particles undergo fragmentation.

The chemical composition of the powders, acquired by both EDS and gas in metal analysis, is shown in Table 2.

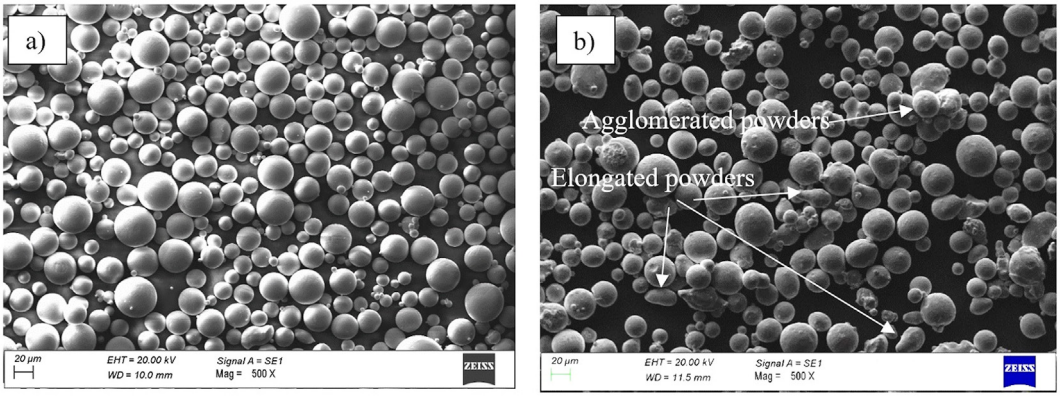

Fig. 3 – SEM image of virgin powders (a) and recycled powders (b).

The amount of alloying elements is about the same in the two types of powders whereas the content of gases is higher in the recycled powders (increase of O ~ 26%, H ~ 50%, C ~ 20%), as expected. An increase of H and O in recycled powders has been also observed by other authors [7,16]. After or during the printing process the powders are in contact with an oxidizing atmosphere, thus increasing the O content. Although the printing process is carried out under an Argon protective atmosphere, the low partial pressure of O (0.2 %vol.) is likely sufficient to produce oxidation of some alloying elements on the surface [19]. Moreover, some pick up of O could also occur during the sieving process, when the powder particles are stirred, and during the powder storage within the machine between two successive jobs, when the Ar saturation progressively decreases. The pick up of O and H in the post printing processing of the powders can be related to a possible pick up of air or moisture from the environment [16] in the same circumstances mentioned above. Finally, the pick up of C can be tentatively attributed to the interaction between the particles and the organic bellows that convey them into the recycling circuit or to the contamination with the process gas impurities. The significant relative variations of C content are related to the small amounts of this element in AISI 316 L stainless steel and thus small contaminations can produce an increase of C content above the maximum level allowed for this alloy.

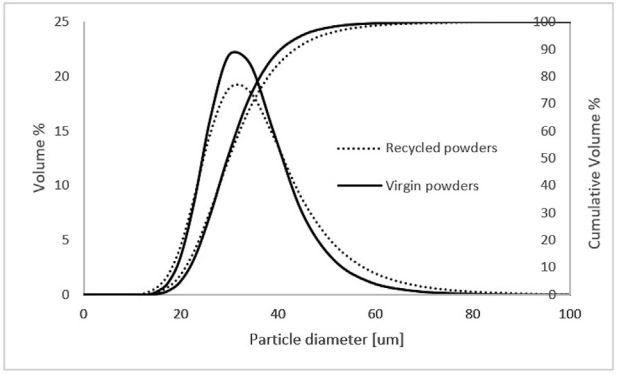

Fig. 5 – Particle size and cumulative distribution for the virgin and recycled powders.

The microstructural characterization shows the presence of austenitic dendrites in the particles of both types of powders (Fig. 6). In the recycled powders, the deposits of the molten metal on the pristine and fragmented particles, that are probably produced by powder breaking during sieving or

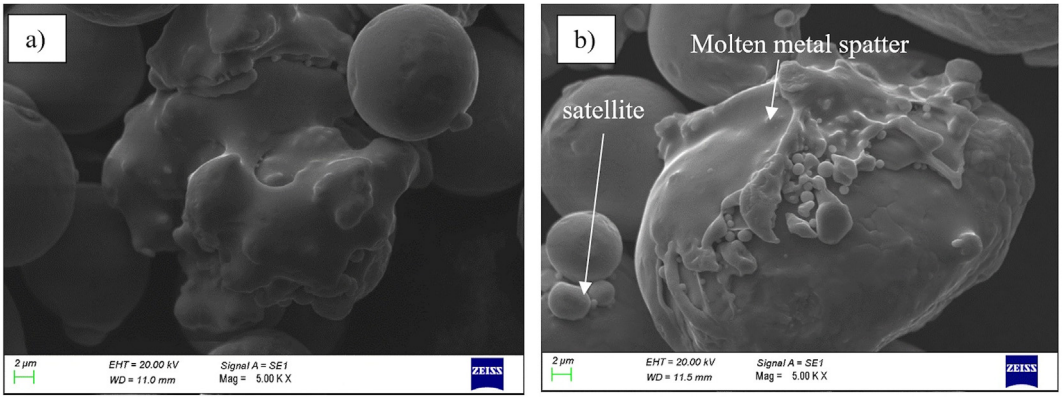

Fig. 4 – SEM images of recycled powders showing particles of irregular shape (a) and particles with satellites and partial coating with metal spatter.

Table 2 – Chemical composition of the analyzed powders [wt%].

	Virgin	Recycled
Cr	17.5 ± 0.4	17.7 ± 0.6
Ni	10.5 ± 0.5	11.0 ± 0.4
Mn	0.8 ± 0.3	0.7 ± 0.2
Mo	2.2 ± 0.5	2.3 ± 0.7
Si	0.7 ± 0.4	0.7 ± 0.3
C	0.027	0.032
S	0.005	0.005
O	0.031	0.038
N	0.099	0.099
H	0.002	0.003

re-coating operations, are well highlighted in Fig. 6 (b). The shape of part of the recycled powders is irregular due to the previous printing processes and, in a minor extent, to reconditioning operations.

A reconstruction of the powder microstructure was done by means of SEM images stitched together (Fig. 7). SEM micrographs confirmed that the particles of recycled powder exhibit an irregular shape. In particular, the image (b) shows two particles stuck together by a molten spatter. Inside the particles of both powders the crystalline grains are decorated by very small non-metallic inclusions, indicated by red points. Fig. 8 shows some sub-micrometric inclusions in a powder particle at high magnification. Owing to the size in the range of few tens of nanometers, the chemical composition of the inclusions could not be easily determined by EDS analysis, although Si and O signals were acquired on the coarser particles (Table 3). The total density of inclusions is slightly higher in the recycled powders (0.87 counts/μm^2) than in the virgin ones (0.79 counts/μm^2). The higher inclusion content of recycled powders is in agreement with the higher O content found in the chemical analysis.

3.2. *Characterization of printed samples*

Table 4 compares the chemical composition of the 3D printed samples with that of the powders used in their manufacturing process.

The chemical composition of 3D printed samples is, within the experimental error, the same of the powders. In agreement with previous results of other investigators [11,26], there is no difference between the chemical composition of samples printed with virgin and recycled powders by considering only the main alloying elements. Possible small differences can be related to partial evaporation of some elements during the

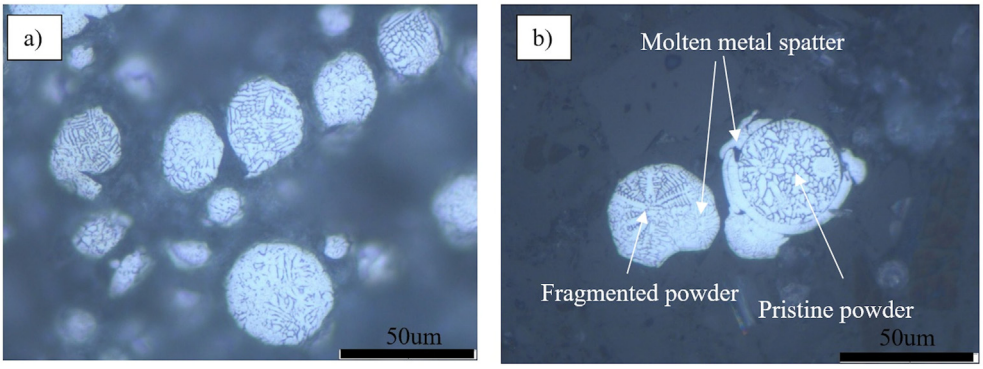

Fig. 6 – Microstructure of virgin (a) and recycled powders (b).

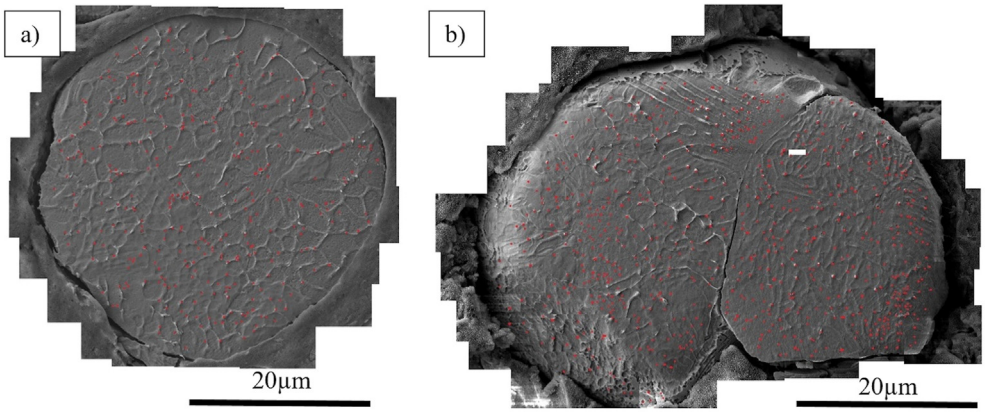

Fig. 7 – FE-SEM images of a single particle of virgin (a) and recycled (b) powder. The red dots indicate the inclusions detected in the material.

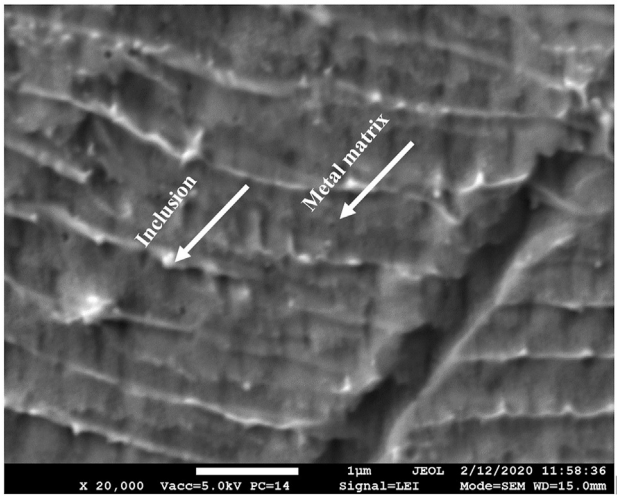

Fig. 8 – FE-SEM representative image of the detected inclusions in recycled powders. EDS analysis reported in Table 3 were collected from the areas indicated by the arrows.

printing process [27]. As it was observed in the analysis of the powders, the only significant differences are related to O and H contents, which are higher in the samples obtained from the recycled powders. Data reported in Table 4 evidence that the recycled powders progressively pick up gases during successive printing jobs, which are transferred to the printed samples.

Samples printed by using both types of powders and built in horizontal and vertical directions have been submitted to a metallographic examination to determine their void size distribution. The results of this analysis are shown in Fig. 9.

There are no relevant differences between the samples built in vertical and horizontal directions with the same batch of powders. However, samples printed with virgin and recycled powders exhibit different void size distributions. In detail, the major part of the voids in the samples printed with virgin powders is of small size (0–20 μm), while the distribution of samples produced with recycled powders presents significant components at 20–40 μm and 40–60 μm. The increase of coarser voids is likely due to the fact that the recycled powders contain a higher amount of gases and present an irregular shape that involves a worse powder flowability with consequent poor powder packing density [5]. Moreover, the chemical modification of the metal powders can affect the laser-material interaction and compromise the efficiency of the printing process. In particular, O increases the laser absorptivity [24] and worsens the material wettability leading to a less stable process [28]. The total void analyses, which were obtained by

Table 3 – Results of the EDS analysis (wt%) in the points indicated by the arrows in Fig. 8.

	Inclusion	Metal matrix
O	1.48	–
Si	0.83	–
Cr	19.9	19.75
Fe	Bal.	Bal.
Ni	14.65	15.25

Table 4 – Chemical composition of the 3D printed samples compared to that of the powders (wt%).

	Virgin		Recycled	
	Powder	Printed	Powder	Printed
Cr	17.5 ± 0.4	17.6 ± 0.5	17.7 ± 0.6	17.8 ± 0.4
Ni	12.5 ± 0.5	12.6 ± 0.3	11.0 ± 0.4	11.7 ± 0.3
Mn	0.8 ± 0.3	0.7 ± 0.2	0.7 ± 0.2	0.8 ± 0.2
Mo	2.2 ± 0.5	2.2 ± 0.4	2.3 ± 0.7	2.3 ± 0.5
Si	0.7 ± 0.4	0.7 ± 0.2	0.7 ± 0.3	0.7 ± 0.3
C	0.027	0.026	0.032	0.030
S	0.005	0.005	0.005	0.005
O	0.031	0.033	0.038	0.040
N	0.099	0.100	0.099	0.098
H	0.002	0.002	0.003	0.003

Archimede' principle weighting, are in agreement with the void size distribution and highlighted a slightly higher pore amount for the samples printed with recycled powder compared to the virgin one (0.11% vs 0.07%). On the other hand, the small sized pores are more related to gas entrapment during the printing process, as observed by other authors [29].

Concerning the microstructural characterization, it is observed that the use of both virgin and recycled powders leads to the same microstructure in the corresponding 3D printed samples. Light microscopy (Fig. 10) shows the presence of melt pools (samples printed in vertical direction) and laser scan paths (samples printed in horizontal direction). At higher magnification (Fig. 11), the typical microstructure of 3D printed AISI 316 L is observed: small columnar austenite grains, which mainly grow perpendicularly to the micro-weld bead borders, and some delta ferrite in the proximity of austenitic grain boundaries. As described in other works (e.g. see Ref. [4]), the microstructure of the material is typical of a supercooling solidification process.

A detailed analysis of the inclusion content was performed on the samples produced with virgin and recycled powders. In this case, only single melt pools of samples printed in the vertical direction were selected from three different positions (high, middle, low) of the sample (Fig. 12 a) for the analysis. In particular, the image of each molten pool was obtained from several images acquired by FE-SEM at high magnification and stitched together (Fig. 12 b). In each melt pool, the small inclusions were detected and highlighted by red dots (Fig. 12 c). These inclusions were counted and normalized with respect to the area of each single melt pool.

The results obtained from inclusion rating analysis are shown in Fig. 13.

Fig. 13 shows that the samples produced with virgin powders present a lower inclusion content than those produced with recycled powders. No differences have been observed between high, middle and low areas of analysis in the same samples suggesting that the inclusion content is not varying during the printing process.

The inclusion content is slightly lower in the powders than in the corresponding printed material. This indicates that the printing process, and in particular the printing atmosphere, is the main cause of oxygen pick up. This would also explain the higher inclusions content of specimens produced with recycled powders, which are richer in O.

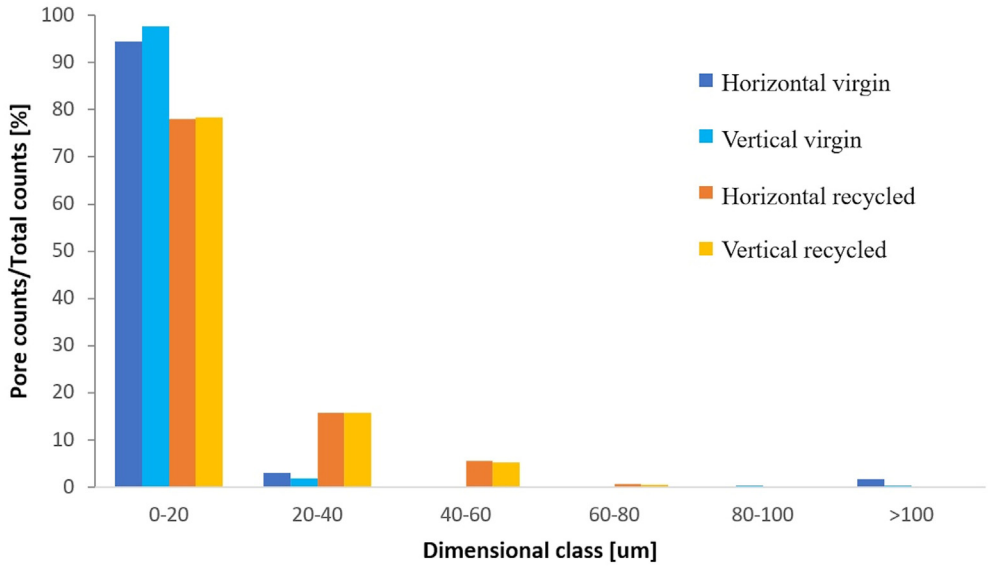

Fig. 9 – Void size distribution in samples printed by using both types of powders and built in horizontal and vertical directions.

It is noteworthy that the increase of inclusion density after the printing process is small in comparison with the inclusion density in the powders used for printing. Indeed, the virgin powders present an inclusion content that is only slightly increased by the process. In particular, the decay of recycled powders in terms of chemical composition and inclusion content is very slow.

The electrochemical extraction of the inclusions was performed to determine their chemical composition, structure and relative amount. The weight fraction of the inclusions resulted to be 0.22 and 0.30 wt% in the samples produced by using virgin and recycled powders, respectively. Both inclusions have similar chemical compositions, which are reported in Table 6, with the presence of Si and O in weight ratio 1:2. Moreover, a small amount of C has been detected only in the inclusions derived from samples which were 3D printed by using recycled powders. Taking into account the C content of the printed samples (Table 4) and of the extracted inclusions (Table 6), the C concentration in the matrix is 0.027 wt %, i.e. the value of the nominal composition of the steel.

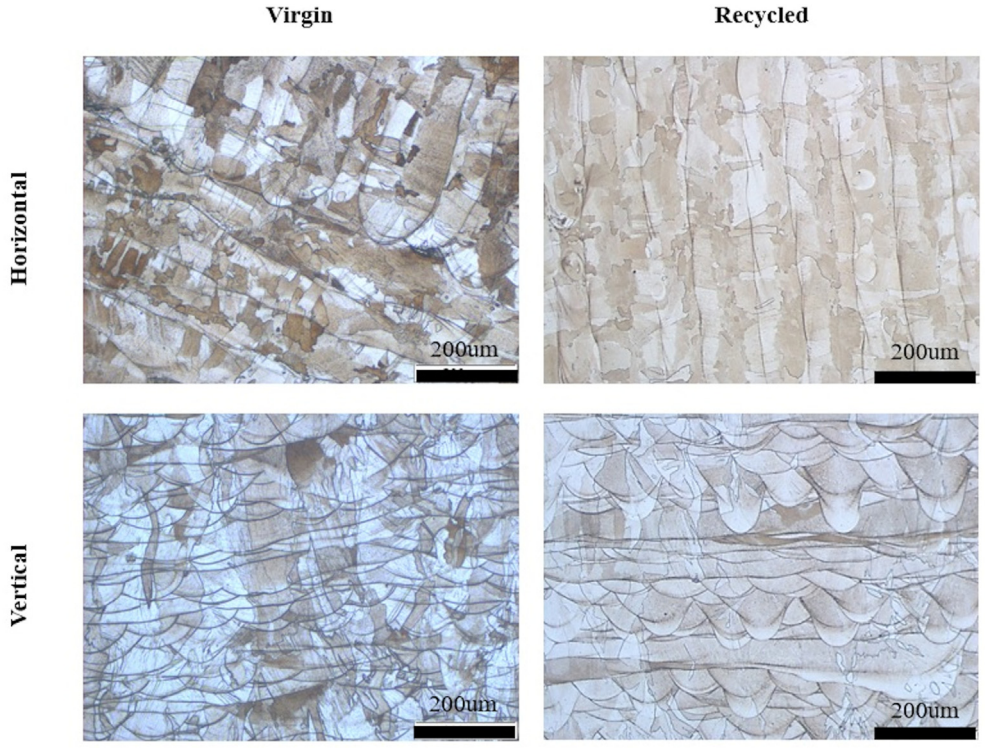

Fig. 10 – Microstructural characterization of 3D printed samples produced with both virgin and recycled powders.

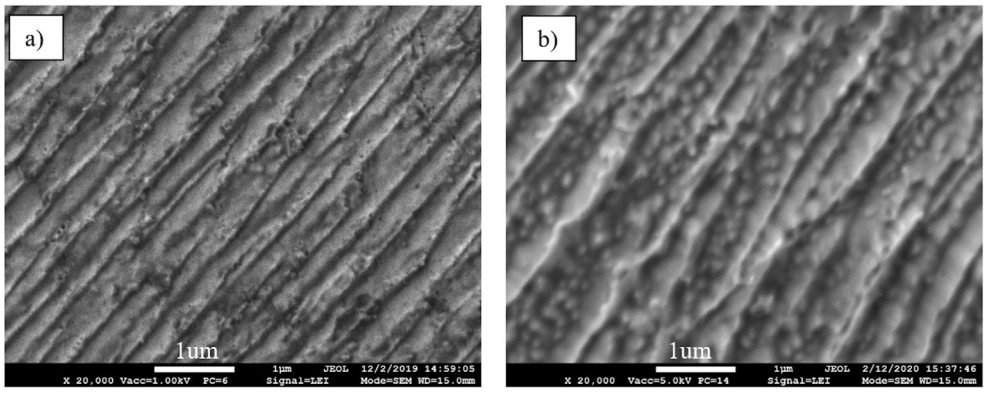

Fig. 11 – FE-SEM images of the microstructure of 3D printed samples produced with virgin (a) and recycled powders (b).

The XRD spectra of the particles extracted from the samples printed using virgin and recycled powders are displayed in Fig. 14.

Both XRD spectra exhibit a pattern with broad maxima, typical of an amorphous material, with peaks related to the crystalline SiO_2 phase (JCPDS file 14-0260; hexagonal structure with lattice parameters a = 9.92 Å and c = 81.5 Å). These results combined with those obtained by EDS (Table 4) indicate that the inclusions consist of mixed amorphous (in major quantity) and crystalline silica.

The weight fractions of inclusions in samples obtained from virgin and recycled powders show that a large part of the inclusions are already present in the virgin powders while only a minor fraction (~0.08 wt%) forms during the repeated printing processes due to the reaction of Si with O. This is also in agreement with SEM observations of the virgin powders (Fig. 7 a) showing a large number of nanometric particles embedded in the metal matrix. Therefore, the gas atomization phase generating new powder particles seems to be the most critical stage of the whole manufacturing process, because a

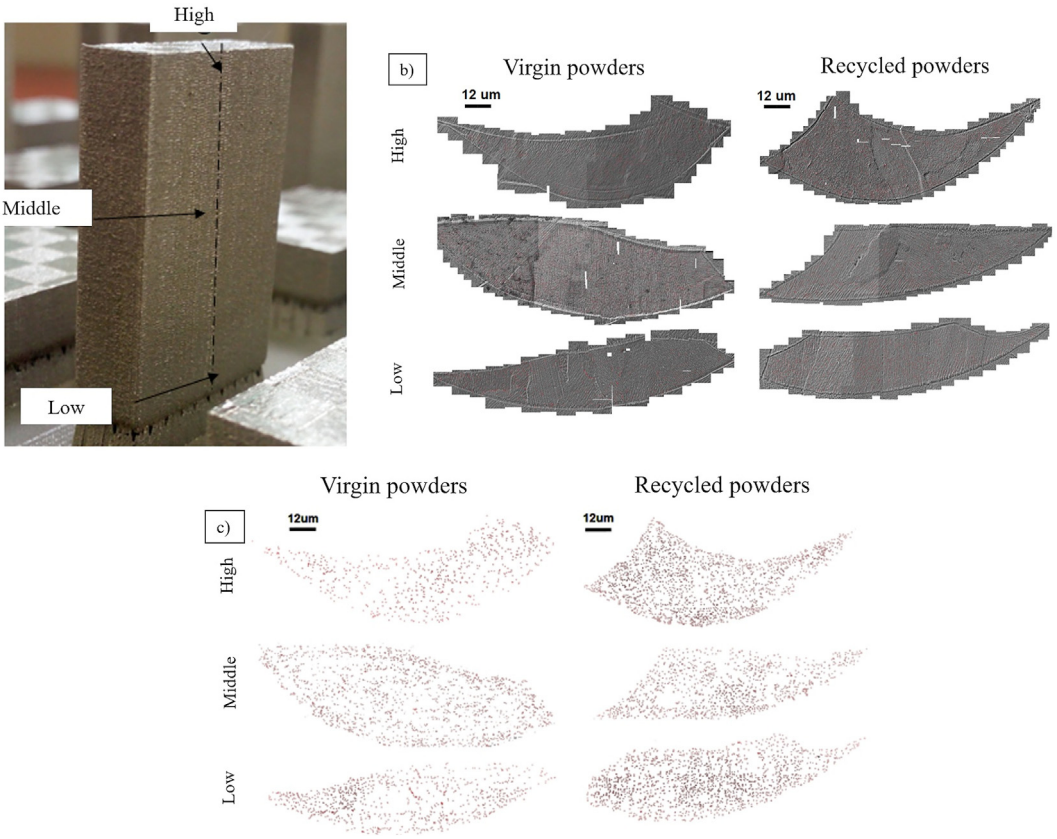

Fig. 12 – Inclusion rating was performed on melt pools at different heights on 3D printed vertical samples (a); FE-SEM images (b); inclusions maps (c). The red dots indicate the inclusions.

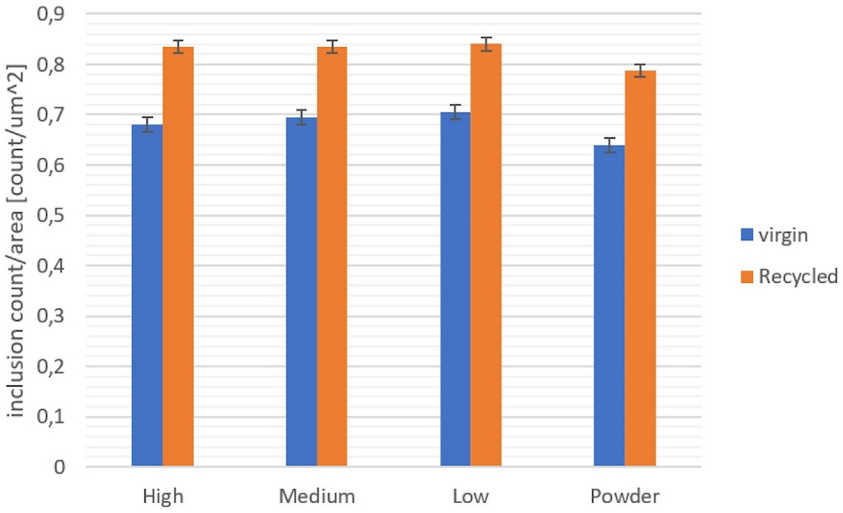

Fig. 13 – Inclusion density acquired from each position of the printed samples shown in Fig. 12 and the powders used in the process.

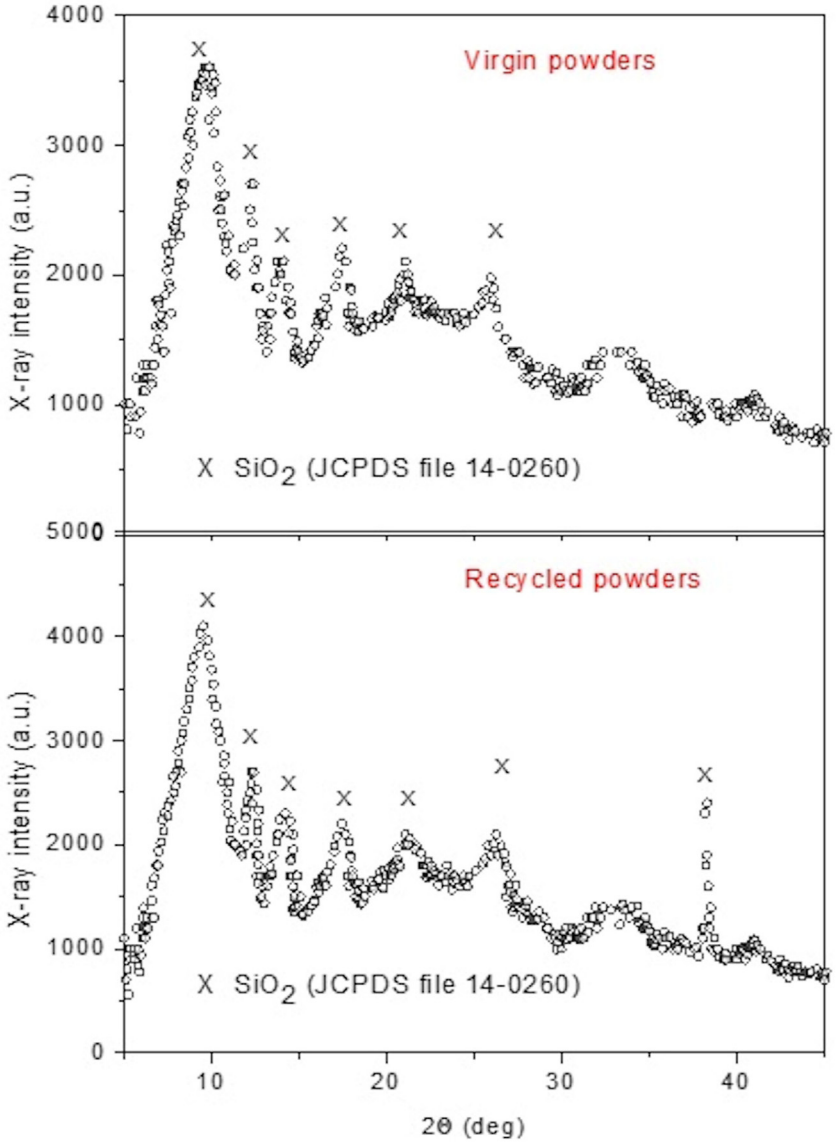

Fig. 14 – XRD spectra of the particles extracted from samples printed with virgin and recycled powders.

Table 5 – Hardness (HV2), yield stress (YS), ultimate tensile strength (UTS) and relative elongation (E) obtained from tensile tests carried out on probes produced with virgin and recycled powders.

Mechanical properties	HV2	YS [MPa] [MPa]	UTS [MPa]	E [%]
Printed by using virgin powders	237 ± 8	494 ± 18	582 ± 20	36 ± 2
Printed by using recycled powders	241 ± 10	530 ± 16	663 ± 23	30 ± 2
Statistical significance (P-value)	0.36	2×10^{-4}	1.19×10^{-7}	2.93×10^{-6}

Table 6 – Chemical composition of the inclusions extracted from samples which were 3D printed using virgin and recycled powders.

Chemical elements (wt%)	Si	O	C
Printed by using virgin powders	33.85 ± 0.82	66.15 ± 2.68	–
Printed by using recycled powders	33.78 ± 0.71	65.16 ± 2.49	1.06 ± 0.29

significant decrease of inclusions number in the printed products can be achieved only through the use of a powder with better quality [30]. This further confirms the recommendations of a recent review paper of Lewis [31], i.e. that a potential area for future research will focus on the optimization of process variables for both the powder production and the powder bed fusion process.

In order to verify possible modification of the mechanical properties of the 3D printed samples using different powder types, hardness and tensile tests were also performed. The results are presented in Table 5.

The values of hardness, YS and UTS of the samples printed using recycled powders are only slightly higher than those of samples printed with virgin powders, while the elongation E is slightly lower. The analysis of variance robustly confirmed the statistical significance of the differences observed for all the investigated parameters, except for hardness values. As pointed out by other authors [8,21], the increase of mechanical properties can be related to the inclusions density, which promotes a sub-micrometric reinforcing effect. Inclusions of small size are pinning points for dislocations hindering their motion under an applied stress and thus leading to material strengthening [32]. On the other hand, the ductility of the material decreases because voids with large size (40–60 μm) are preferential sites for crack nucleation. It is important to highlight that the possible negative effect of the high density of voids on elongation is compensated by the high amount of inclusions and voids with sub-micrometric size that increase the YS and UTS. Concerning the hardness results, the negligible variation between the two tested batches is in agreement with other works found in literature [14].

4. Conclusions

Virgin and recycled AISI 316 L powders, and the corresponding 3D printed samples obtained by L-PBF process were investigated in this work. The main conclusions can be summarized as follows.

1. Recycled powders show an irregular shape due to fragmentation, spatters and satellites. These are the result of the interaction of the powder particles with molten metal combined with mechanical stresses experienced during repeated printing operations. Recycled powders display a higher gas content (O, H and C) and amount of surface oxides than virgin ones.
2. Virgin and recycled powders contain non-metallic inclusions with a higher inclusion content in the latter.
3. The microstructure of samples produced from virgin and recycled powders is similar. Nevertheless, samples produced using recycled powders exhibit voids with larger size due to their higher amount of gases in the powders and their irregular shape.
4. Several inclusions were observed in samples printed with virgin and recycled powders. Their amount is slightly higher for samples produced with recycled powders. The inclusion content is not significantly varying in the different regions that were characterized in the samples.
5. The samples produced with recycled powders present slightly higher mechanical properties (YS, UTS) than those printed with virgin powders. This is associated with a slight decrease of ductility (E%) for samples produced with recycled powders. It is likely that the presence of a high density of voids, that are responsible of the ductility loss, is compensated by the high amount of sub-micrometric inclusions that increase the mechanical properties of the printed material.
6. XRD and EDS examinations of the inclusions extracted from the metallic matrix showed that they consist of a mix of amorphous (in major quantity) and crystalline silica. Large part of these particles are already present in the virgin powders, while only a minor fraction forms during repeated printing operations.
7. The most important factor controlling the inclusion content of AM products is the quality of the virgin powders. As a consequence, powder production should be considered the most critical stage of the whole manufacturing process.

Declaration of competing interest

The authors declare that they have no known competing financial interests or personal relationships that could have appeared to influence the work reported in this paper.

Acknowledgements

The authors are grateful to Acciaierie Fonderie Cividale (Mr. M. Zuliani and his team) for the gas in metal analyses as well as to Horiba, Ltd. and Horiba Techno Service Co., Ltd. for the use of the EMIA-Expert and EMGA-930 trace element analytical instruments.

REFERENCES

[1] Mower TM, Long MJ. Mechanical behavior of additive manufactured, powder-bed laser-fused materials. Mater Sci Eng 2016;651:198–213. https://doi.org/10.1016/j.msea.2015.10.068.

[2] Revilla RI, Wouters B, Andreatta F, Lanzutti A, Fedrizzi L, De Graeve I. EIS comparative study and critical Equivalent Electrical Circuit (EEC) analysis of the native oxide layer of additive manufactured and wrought 316L stainless steel. Corros. Sci. 2020;167. https://doi.org/10.1016/j.corsci.2020.108480.

[3] Andreatta F, Lanzutti A, Vaglio E, Totis G, Sortino M, Fedrizzi L. Corrosion behaviour of 316L stainless steel manufactured by selective laser melting. Mater Corros 2019;70. https://doi.org/10.1002/maco.201910792.

[4] Lanzutti A, Marin E, Tamura K, Morita T, Magnan M, Vaglio E, et al. High temperature study of the evolution of the tribolayer in additively manufactured AISI 316L steel. Addit Manuf 2020;34:101258. https://doi.org/10.1016/j.addma.2020.101258.

[5] Leung CLA, Marussi S, Towrie M, Atwood RC, Withers PJ, Lee PD. The effect of powder oxidation on defect formation in laser additive manufacturing. Acta Mater 2019;166:294–305. https://doi.org/10.1016/j.actamat.2018.12.027.

[6] Powell D, Rennie AEW, Geekie L, Burns N. Understanding powder degradation in metal additive manufacturing to allow the upcycling of recycled powders. J Clean Prod 2020;268:122077. https://doi.org/10.1016/j.jclepro.2020.122077.

[7] Lu C, Zhang R, Xiao M, Wei X, Yin Y, Qu Y, et al. A comprehensive characterization of virgin and recycled 316L powders during laser powder bed fusion. J Mater Res Technol 2022;18:2292–309. https://doi.org/10.1016/j.jmrt.2022.03.125.

[8] Saboori A, Aversa A, Bosio F, Bassini E, Librera E, De Chirico M, et al. An investigation on the effect of powder recycling on the microstructure and mechanical properties of AISI 316L produced by Directed Energy Deposition. Mater Sci Eng 2019;766:138360. https://doi.org/10.1016/j.msea.2019.138360.

[9] Sehhat M, Sutton A, Leu M. Enhancement of gas-atomized 304L stainless steel powder by plasma spheroidization for use in the laser powder bed fusion. Process 2022;1. https://doi.org/10.2172/1876883.

[10] Heiden MJ, Deibler LA, Rodelas JM, Koepke JR, Tung DJ, Saiz DJ, et al. Evolution of 316L stainless steel feedstock due to laser powder bed fusion process. Addit Manuf 2019;25:84–103. https://doi.org/10.1016/j.addma.2018.10.019.

[11] Sutton AT, Kriewall CS, Leu MC, Newkirk JW, Brown B. Characterization of laser spatter and condensate generated during the selective laser melting of 304L stainless steel powder. Addit Manuf 2020;31:100904. https://doi.org/10.1016/j.addma.2019.100904.

[12] Lu C, Zhang R, Wei X, Xiao M, Yin Y, Qu Y, et al. An investigation on the oxidation behavior of spatters generated during the laser powder bed fusion of 316L stainless steel. Appl Surf Sci 2022;586:152796. https://doi.org/10.1016/j.apsusc.2022.152796.

[13] Pinto FC, Souza Filho IR, Sandim MJR, Sandim HRZ. Defects in parts manufactured by selective laser melting caused by δ-ferrite in reused 316L steel powder feedstock. Addit Manuf 2020;31:100979. https://doi.org/10.1016/j.addma.2019.100979.

[14] Delacroix T, Lomello F, Schuster F, Maskrot H, Garandet JP. Influence of powder recycling on 316L stainless steel feedstocks and printed parts in laser powder bed fusion. Addit Manuf 2022;50. https://doi.org/10.1016/j.addma.2021.102553.

[15] Eo DR, Park SH, Cho JW. Inclusion evolution in additive manufactured 316L stainless steel by laser metal deposition process. Mater Des 2018;155:212–9. https://doi.org/10.1016/j.matdes.2018.06.001.

[16] Deng P, Karadge M, Rebak RB, Gupta VK, Prorok BC, Lou X. The origin and formation of oxygen inclusions in austenitic stainless steels manufactured by laser powder bed fusion. Addit Manuf 2020;35:101334. https://doi.org/10.1016/j.addma.2020.101334.

[17] Yan F, Xiong W, Faierson E, Olson GB. Characterization of nano-scale oxides in austenitic stainless steel processed by powder bed fusion. Scripta Mater 2018;155:104–8. https://doi.org/10.1016/j.scriptamat.2018.06.011.

[18] Chao Q, Cruz V, Thomas S, Birbilis N, Collins P, Taylor A, et al. Scripta Materialia on the enhanced corrosion resistance of a selective laser melted austenitic stainless steel. Scripta Mater 2017;141:94–8. https://doi.org/10.1016/j.scriptamat.2017.07.037.

[19] Pauzon C, Hryha E, Forêt P, Nyborg L. Effect of argon and nitrogen atmospheres on the properties of stainless steel 316 L parts produced by laser-powder bed fusion. Mater Des 2019;179. https://doi.org/10.1016/j.matdes.2019.107873.

[20] Lou X, Andresen PL, Rebak RB. Oxide inclusions in laser additive manufactured stainless steel and their effects on impact toughness and stress corrosion cracking behavior. J Nucl Mater 2018;499:182–90. https://doi.org/10.1016/j.jnucmat.2017.11.036.

[21] Cordova L, Campos M, Tinga T. Revealing the effects of powder reuse for selective laser melting by powder characterization. JOM (J Occup Med) 2019;71:1062–72. https://doi.org/10.1007/s11837-018-3305-2.

[22] Pelegatti M, Benasciutti D, De Bona F, Lanzutti A, Magnan M, Srnec Novak J, et al. On the factors influencing the elastoplastic cyclic response and low cycle fatigue failure of AISI 316L steel produced by laser-powder bed fusion. Int J Fatig 2022;165:107224. https://doi.org/10.1016/j.ijfatigue.2022.107224.

[23] JCPDS-International Centre for Diffraction Data, Newtown square, PA 19073, USA. JCPDS-international centre for diffraction data, newtown square, PA 19073, USA., (n.d.) 19073.

[24] Fedina T, Sundqvist J, Kaplan AFH. Spattering and oxidation phenomena during recycling of low alloy steel powder in Laser Powder Bed Fusion. Mater Today Commun 2021;27:102241. https://doi.org/10.1016/j.mtcomm.2021.102241.

[25] Wang D, Ye G, Dou W, Zhang M, Yang Y, Mai S. Influence of spatter particles contamination on densification behavior and tensile properties of CoCrW manufactured by selective laser melting. Opt Laser Technol 2020;121:105678. https://doi.org/10.1016/j.optlastec.2019.105678.

[26] Sutton AT, Kriewall CS, Karnati S, Leu MC, Newkirk JW, Everhart W, et al. Evolution of AISI 304L stainless steel part properties due to powder recycling in laser powder-bed fusion. Addit Manuf 2020;36:101439. https://doi.org/10.1016/j.addma.2020.101439.

[27] Murkute P, Pasebani S, Isgor OB. Production of corrosion-resistant 316L stainless steel clads on carbon steel using powder bed fusion-selective laser melting. J Mater Process Technol 2019;273:116243. https://doi.org/10.1016/j.jmatprotec.2019.05.024.
[28] Das S. Physical aspects of process control in selective laser sintering of metals. Adv Eng Mater 2003;5:701–11. https://doi.org/10.1002/adem.200310099.
[29] Liverani E, Toschi S, Ceschini L, Fortunato A. E ff ect of selective laser melting (SLM) process parameters on microstructure and mechanical properties of 316L austenitic stainless steel. J Mater Process Technol 2017;249:255–63. https://doi.org/10.1016/j.jmatprotec.2017.05.042.
[30] Sehhat MH, Sutton AT, Hung CH, Newkirk JW, Leu MC. Investigation of mechanical properties of parts fabricated with gas- and water-atomized 304L stainless steel powder in the laser powder bed fusion process. JOM (J Occup Med) 2022;74:1088–95. https://doi.org/10.1007/s11837-021-05029-7.
[31] Lewis G. Aspects of the powder in metal additive manufacturing: a review. World J Eng Technol 2022;10:363–409. https://doi.org/10.4236/wjet.2022.102022.
[32] Zhong Y, Liu L, Zou J, Li X, Cui D, Shen Z. Oxide dispersion strengthened stainless steel 316L with superior strength and ductility by selective laser melting. J Mater Sci Technol 2020;42:97–105. https://doi.org/10.1016/j.jmst.2019.11.004.